Supporting Information

Visible Light-Responsive Self-Healing Polyurea Elastomers Driven by Dynamic Coordination for Underwater and Low-Temperature Applications

Jingyi Liu[a], Hui Li[*a], Yuanpeng Wu[*a,b], Chunxia Zhao[a], Jinbo Cheng[a], Haoran Huang[a], Yijin Zhang[a]

[a] Sichuan Chongqing Joint Key Lab Green Hydrogen Pro, School of New Energy and Materials, Southwest Petroleum University, Chengdu 610500, China

[b] State Key Laboratory of Oil and Gas Reservoir Geology and Exploitation, Southwest Petroleum University, Chengdu 610500, China

Experimental

Synthesis of 4-((5-methoxybenzo[d]thiazol-2-yl)diazenyl)phenol (PDB-OH)

The PDB-OH was prepared according to the literature with some modifications. 2-Amino-6-methoxybenzothiazole (5.0 g, 27.6 mmol) was charged into a 500 mL round-bottom flask immersed in an ice bath. Glacial acetic acid (125 mL) and sulfuric acid (60%, 100 mL) were added, and the mixture was stirred at 350 rpm. Upon temperature stabilization, an aqueous solution of sodium nitrite (1.9 g in 62.5 mL water) was added dropwise. The reaction mixture was stirred for 1 h to ensure complete diazotization. Subsequently, a solution of phenol (2.6 g, 27.6 mmol) in ethanol (75 mL) was added dropwise to the system. After stirring for an additional 1 h, the pH of the reaction mixture was adjusted to 6-7 using a 1.0 M NaOH aqueous solution. The resulting precipitate was collected by vacuum filtration, washed thoroughly

with deionized water, and dried to yield the target benzothiazole-azo phenol as a red solid.

Synthesis of 3-(4-((5-methoxybenzo[d]thiazol-2-yl)diazenyl)phenoxy)propan-1-amine (PDB-NH_2)

tert-Butyl (3-chloropropyl)carbamate (3.05 g, 15.7 mmol) was dissolved in DMF (30 mL) in a 100 mL round-bottom flask. PDB-OH (3.0 g, 10.0 mmol), potassium carbonate (K_2CO_3, 1.74 g), and potassium iodide (KI, 0.35 g) were subsequently added to the solution. The reaction mixture was stirred at 350 rpm and heated at 80℃ for 12 h. After cooling to room temperature, the mixture was diluted with water and extracted with dichloromethane (DCM). The combined organic layer was dried over anhydrous sodium sulfate (Na_2SO_4) and concentrated under reduced pressure to obtain a wine-red liquid. The crude product was purified by silica gel column chromatography (eluent: petroleum ether/ethyl acetate = 1:4 v/v) to afford the Boc-protected target product, PDB-NHBoc, as a purple-red solid.

The PDB-NHBoc (0.7 g, 1.58 mmol) was placed in a 25 mL round-bottom flask. A mixture of trifluoroacetic acid (TFA) and dichloromethane (DCM) (15.6 mL, 1:5 v/v) was added to the flask. The reaction mixture was stirred at room temperature for 3 h. Subsequently, the solvent and excess volatiles were removed under reduced pressure. The crude residue was purified by silica gel column chromatography (eluent: DCM/methanol = 1:4 v/v) to afford the target product, PDB-NH_2, as a dark red solid.

Characterization

^{1}H nuclear magnetic resonance (^{1}H NMR) spectra were recorded on a Bruker AVANCE III HD 400 MHz NMR spectrometer at 25°C with 64 scans. Fourier transform infrared (FTIR) spectroscopy measurements were performed on a Thermo Scientific Nicolet 6700 instrument in the wavenumber range of 400 to 4000 cm^{-1}.The surface temperature of the membrane is measured using a temperature sensor (OMEGA RDXL4SD). The infrared thermal imaging was

captured using VanoCam-HD research980 at a frequency of 1 second. Ultraviolet–visible (UV–vis) absorption spectroscopy measurements were performed on a Shimadzu UV-2600 spectrometer in the wavelength range of 200 to 800 nm, using sample solutions with a concentration of 1×10^{-4} mol/L. The *trans–cis* isomerization content was calculated using the following formula:

$$Tans\text{ - }Azo\ content = \frac{P_t}{P_0} \times 100\% \#(1)$$

where P_t is the peak intensity of the test and P_0 is the initial peak intensity.

Density functional theory (DFT) calculations were performed using the DMol[3] module of Materials Studio 2020[1, 2]. The Perdew–Burke–Ernzerhof (PBE) functional within the generalized gradient approximation (GGA) was employed to calculate the exchange–correlation potential. A full electron double numerical basis set including d and p polarization functions (DNP) was adopted in the calculations. The convergence criteria for geometry optimization were set as follows: energy tolerance = 1.0×10^{-4} Ha/atom, maximum force tolerance = 0.02 Ha/Å, and maximum displacement tolerance = 0.05 Å; all structures were fully optimized.

X-ray absorption fine structure (XAFS) measurements were carried out at the RapidXAFS1M beamline; the duration of a single scan was 123 min. The differential scanning calorimetry test was conducted using TA Q20, with the temperature range set from -80 to 100°C and the heating rate at 10°C/min. The second heating curve was selected. Stress–strain curves were measured using a universal testing machine(CMT 4104) at a stretching rate of 100 mm/min.

Self-healing procedures of PSHA-Zn

To test the photoresponsive self-healing ability of the film, its surface was scratched using a blade, and the film was carefully reassembled at the scratched site. The scratched film was exposed to 450 nm and 550 nm light sources. Both wavelengths were emitted from dual interfaces of the same irradiation equipment, providing a consistent light intensity of approximately 200

mW/cm^2. To ensure high reproducibility and comparability across different testing scenarios, the precise distance between the light source and the polymer specimens was strictly maintained at ~10 cm for all experiments. The healing efficiency was calculated using the following equation:

$$\varphi = \frac{\sigma_t}{\sigma_0} \times 100\% \#(2)$$

where σ_0 and σ_t are the strengths or Strain of the film before and after healing, respectively. All mechanical tensile tests and self-healing efficiency evaluations were performed using at least 3 independent parallel specimens for each condition.

Supportting Figures and Tables

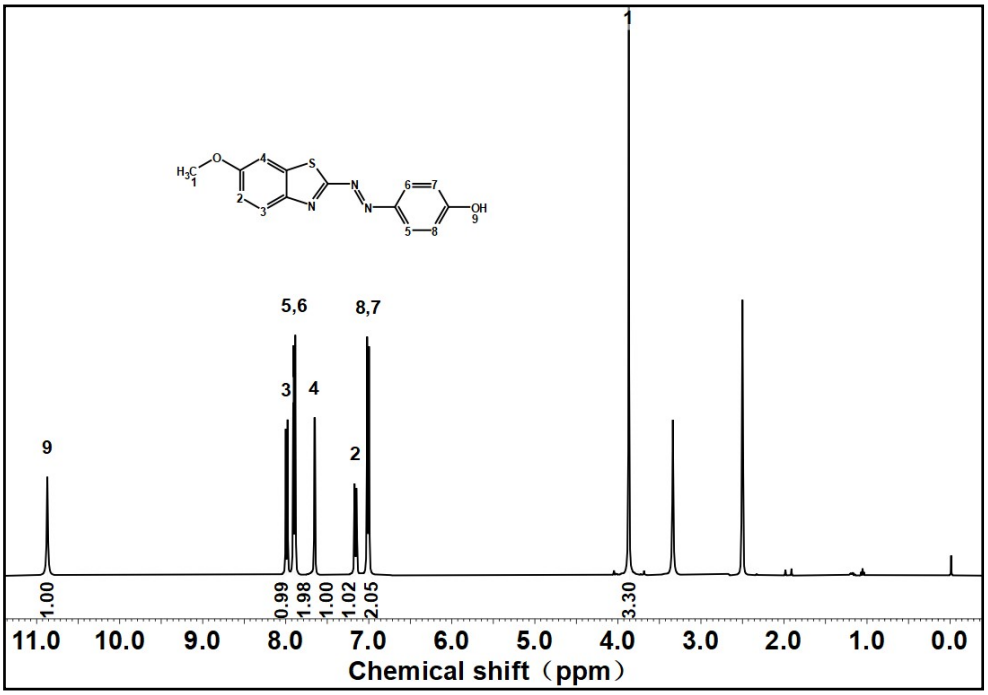

Figure S1. The ^{1}HNMR spectrum of PDB-OH.

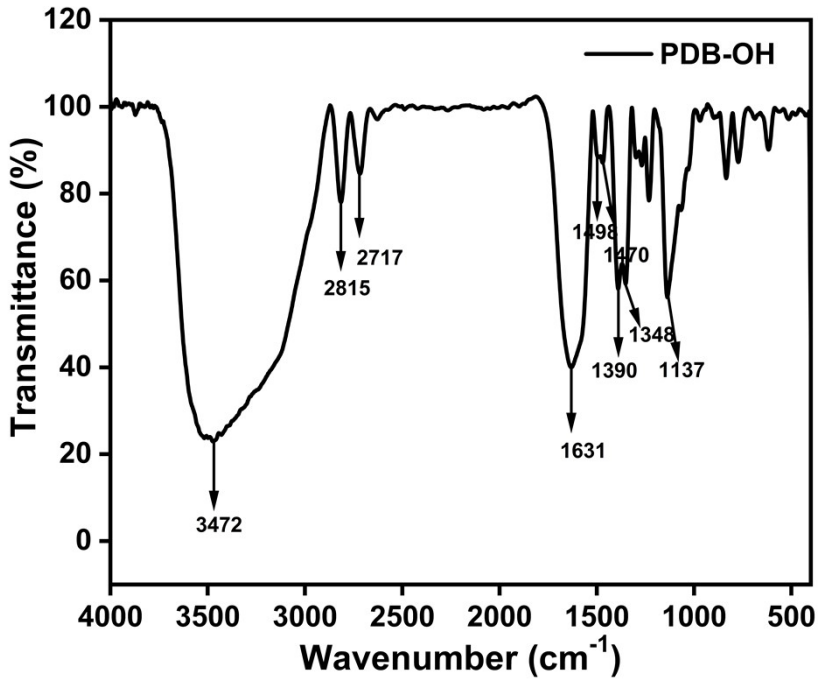

Figure S2. The FT-IR spectrum of PDB-OH.

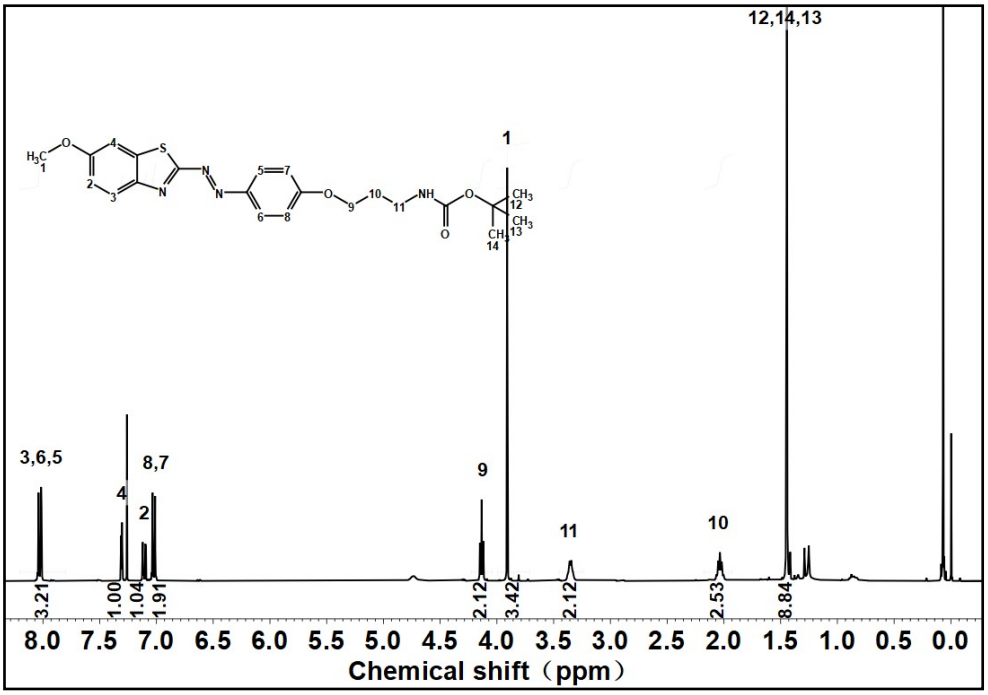

Figure S3. The ^{1}HNMR spectrum of Boc-PDB-NH_2.

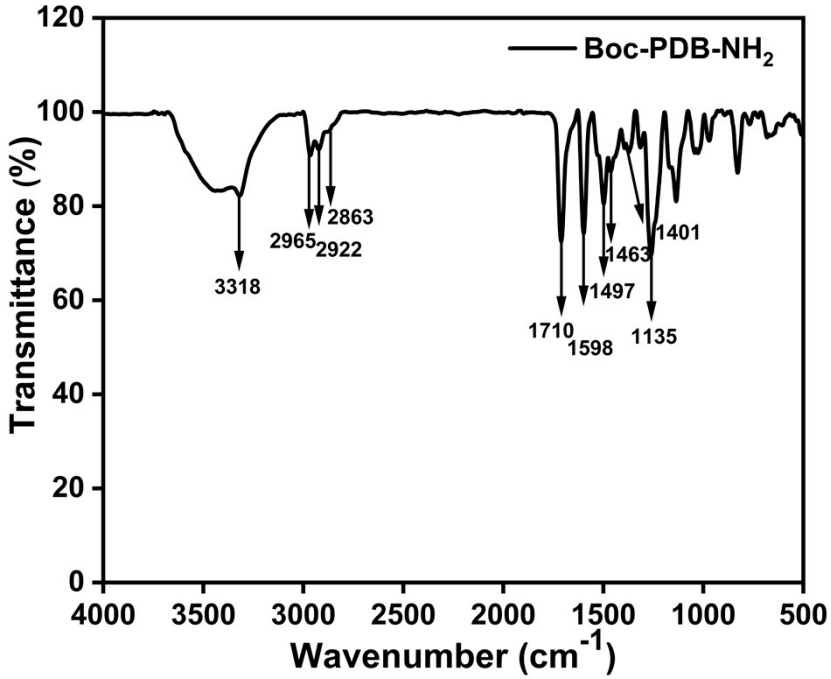

Figure S4. The FT-IR spectrum of Boc-PDB-NH_2.

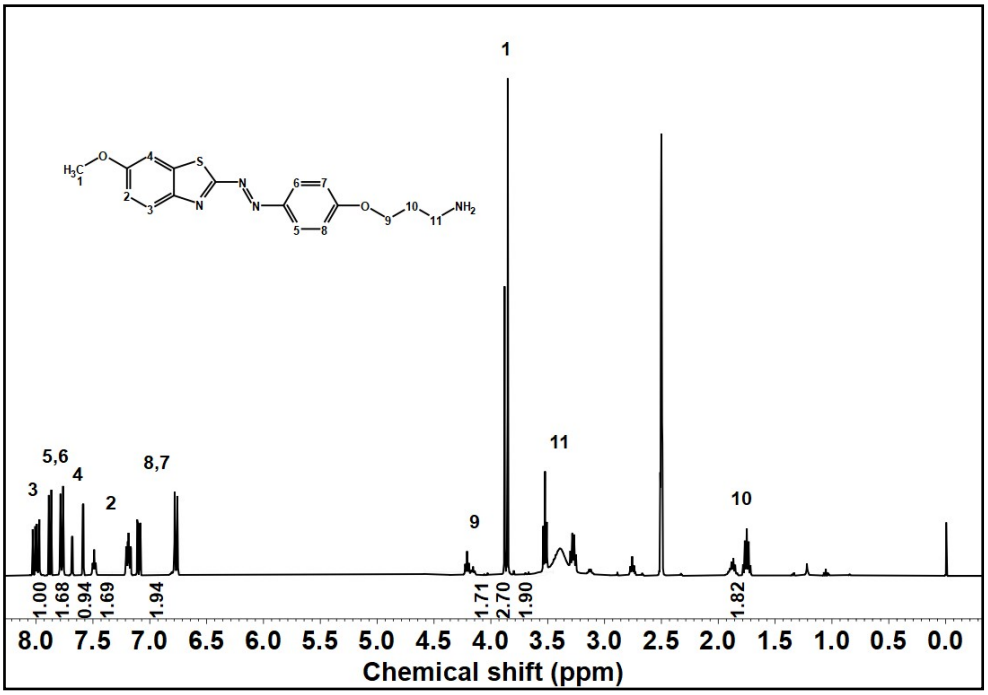

Figure S5. The ^{1}HNMR spectrum of PDB-NH_2.

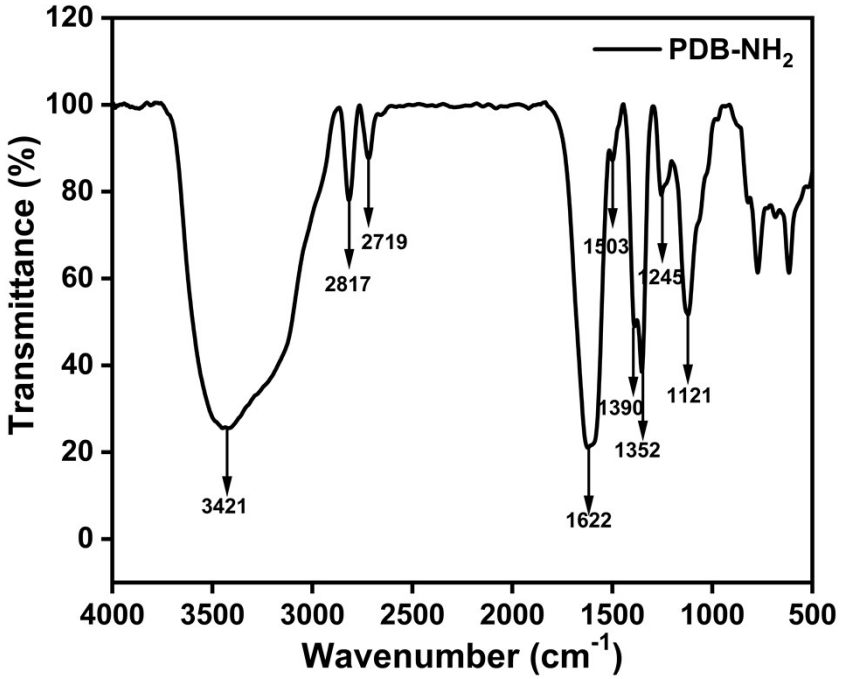

Figure S6. The FT-IR spectrum of PDB-NH_2.

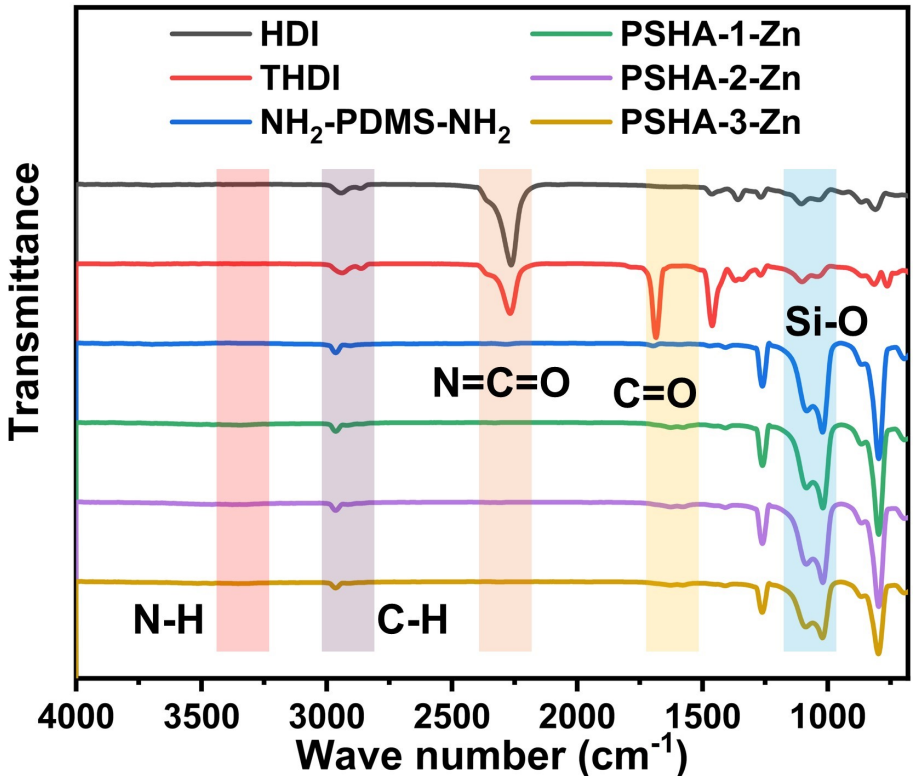

Figure S7. FT-IR spectrum of HDI, THDI, NH2-PDMS-NH2, PSHA-1-Zn, PSHA-2-Zn, and PSHA-3-Zn.

Table S1. The synthesis formula of PSHA-Zn.

Sample	THDI	HDI	PDMS	PDB-NH_2	Zn^{2+}
PSHA-1-Zn	0.05	1.275	1.2	0.3	0.15
PSHA-2-Zn	0.1	1.2	1.2	0.3	0.15
PSHA-3-Zn	0.15	1.125	1.2	0.3	0.15

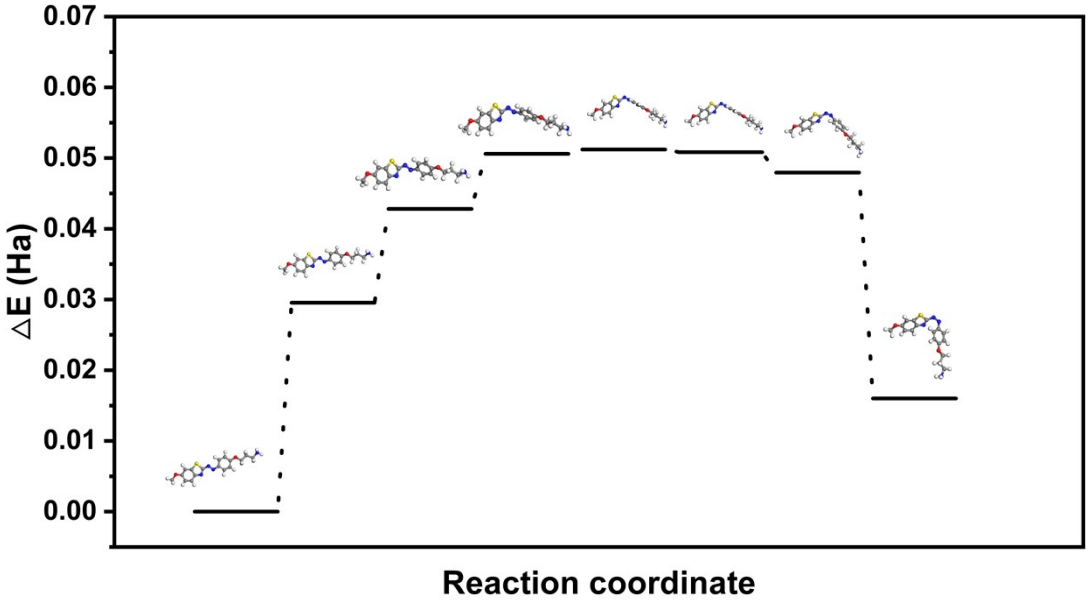

Figure S8. Calculation of the photo-induced isomerization transition state of PDB-NH_2.

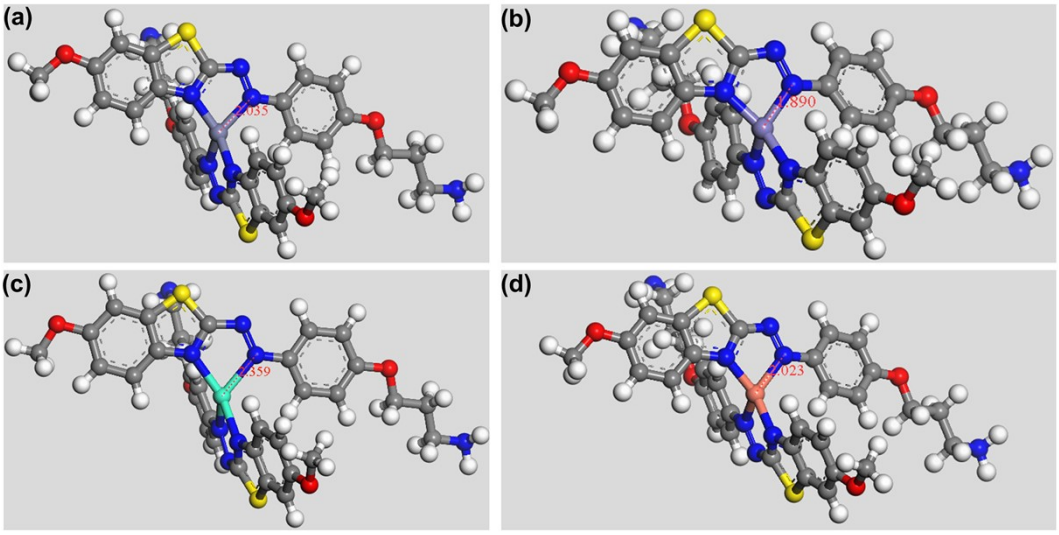

Figure S9. Coordination models of various metal ions with PDB-NH_2. (a) Zn^{2+} (b) Fe^{3+} (c) Tb^{3+} (d) Cu^{2+}.

Table S2. Table of coordination energy calculation data for different metal ions with

PDB-NH_2.

Metal ions	Total energy(Ha)	Metal atomic energy(Ha)	The remaining energy(Ha)	Coordination energy(Ha)	Bond length(Å)
Zn	-4629.701748	-1779.173836	-2850.383168	0.1447447	2.035
Fe	-4114.127229	-1263.445137	-2850.358618	0.3234739	1.890
Tb	-14079.91559	-11229.87269	-2849.807361	0.2355358	2.359
Cu	-4490.88596	-1640.291717	-2850.389901	0.2043421	2.023

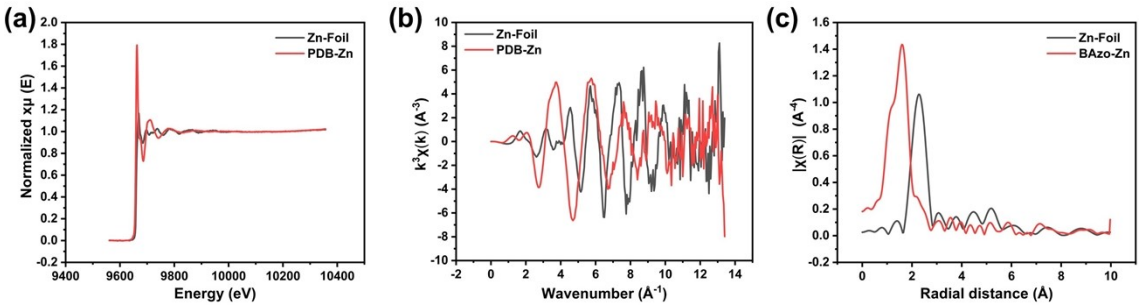

Figure S10. PDB-Zn and the corresponding Zn-Foil XANES spectra (a) Normalized E-space spectrum, (b) k-space spectrum, (c) R-space spectrum.

Table S3. EXAFS fitting data table of the PDB-Zn.

PDB-Zn fit	
Coordination number	4
Coordination bond length(Å)	2.09147
σ^2(Å)	0.01063
ΔE_0(eV)	1.638
R-factor	0.0149659

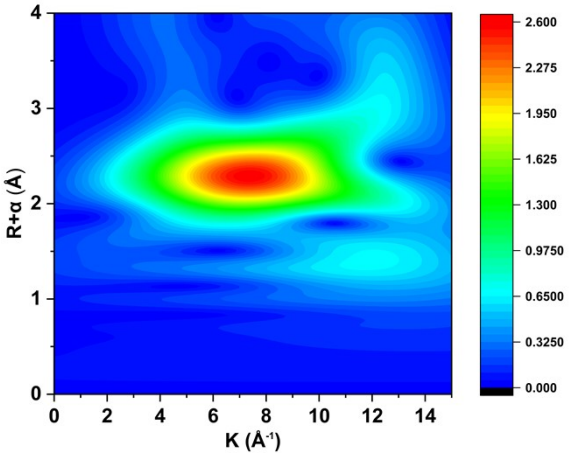

Figure S11. Wavelet transform EXAFS spectrum of PDB-Zn.

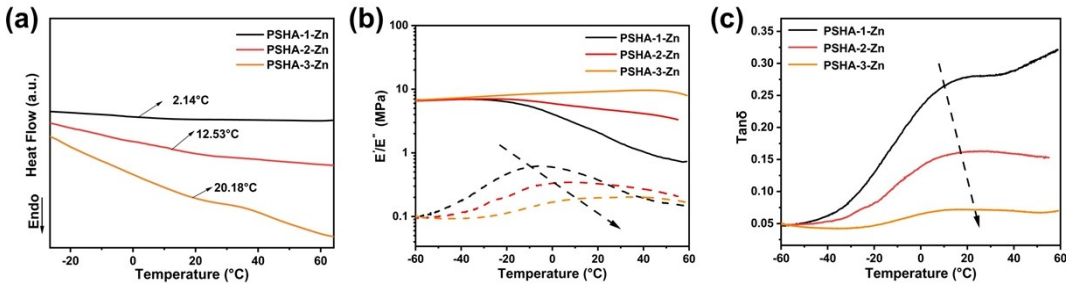

Figure S12. The DSC and DMA curves of PSHA with different THDI contents.

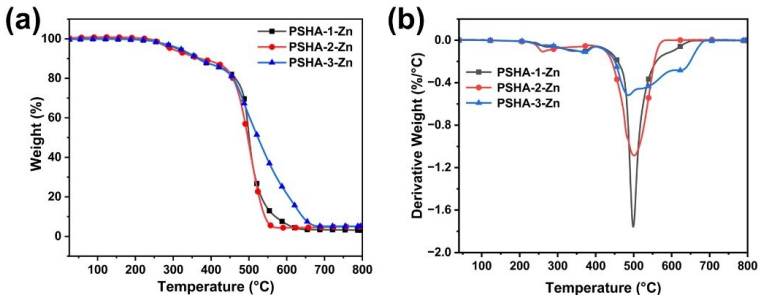

Figure S13. The TGA (a) and DTG (b) curves of PSHA with different THDI contents.

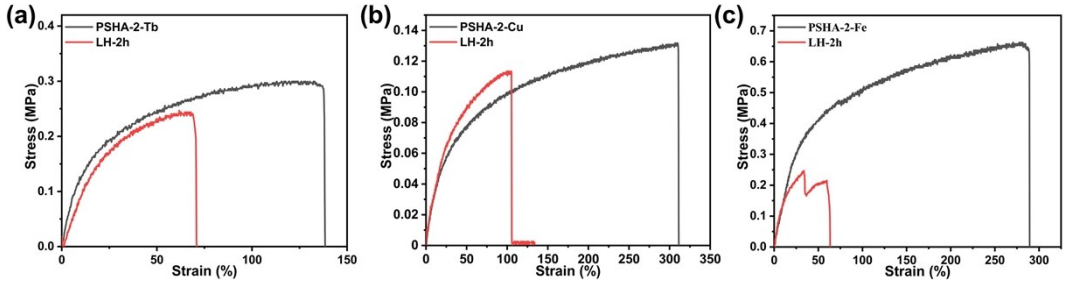

Figure S14. Stress-strain curves of PSHA before and after healing with different metal ions coordination(a) Tb^{3+} (b) Cu^{2+}. (c) Fe^{3+}.

Table S4. Detailed mechanical data and self-healing efficiency under different conditions of the three PSHA-Zn types.

Sample	Tensile Stress (MPa)	Tensile Strain (%)	Fracture toughness (MJ/m^3)	Strength healing efficiency(%)	Strain healing efficiency（%）	Toughness healing efficiency(%)
PSHA-1-Zn	0.38 ± 0.02	266.2 ± 13.3	91.02 ± 5.4	-	-	
LH-2h	0.36 ± 0.03	82.8 ± 3.4	24.95 ± 1.2	96.1 ± 6.7	31.0 ± 1.2	27.4 ± 2.4
LH-4h	0.37 ± 0.01	133.5 ± 8.0	41.87± 0.84	98.9 ± 7.9	50.1 ± 1.5	46.0 ± 2.7
LH-8h	0.37 ± 0.02	212.4 ± 8.5	72.82 ± 6.55	97.9 ± 4.9	79.8 ± 6.3	80.0 ± 2.4
PSHA-2-Zn	0.43 ± 0.02	415.6 ± 29.0	130.81 ± 3.9	-	-	
LH-1h	0.37 ± 0.01	253.4 ± 12.6	66.49 ± 5.3	86.3 ± 1.7	61.0 ± 5.4	50.8 ± 2.0
LH-2h	0.45 ± 0.01	398.3 ± 23.9	119.78 ± 4.7	103.3 ± 7.2	95.8 ± 4.7	91.5 ± 7.3
SH 2h	0.44 ± 0.02	392.0 ± 31.3	123.29 ± 2.4	102.9 ± 4.1	94.3 ± 8.4	94.2 ± 5.6
PSHA-3-Zn	0.78 ± 0.07	786.7 ± 23.6	385.82 ± 27.0	-	-	
LH-2h	0.38 ± 0.01	245.0 ± 4.9	125.02 ± 6.2	48.7 ± 3.9	31.8 ± 0.9	32.4 ± 2.2
LH-4h	0.50 ± 0.05	355.8 ± 14.2	176.97 ± 14.1	64.4 ± 1.2	45.2 ± 2.7	45.8 ± 2.2
LH-8h	0.60 ± 0.02	491.7 ± 34.4	208.18 ± 10.4	76.9 ± 6.1	62.5 ± 2.5	53.9 ± 4.8
LH-12h	0.76 ± 0.04	747.5 ± 14.9	349.47 ± 20.9	97.6 ± 2.9	98.0 ± 6.8	90.5 ± 3.6

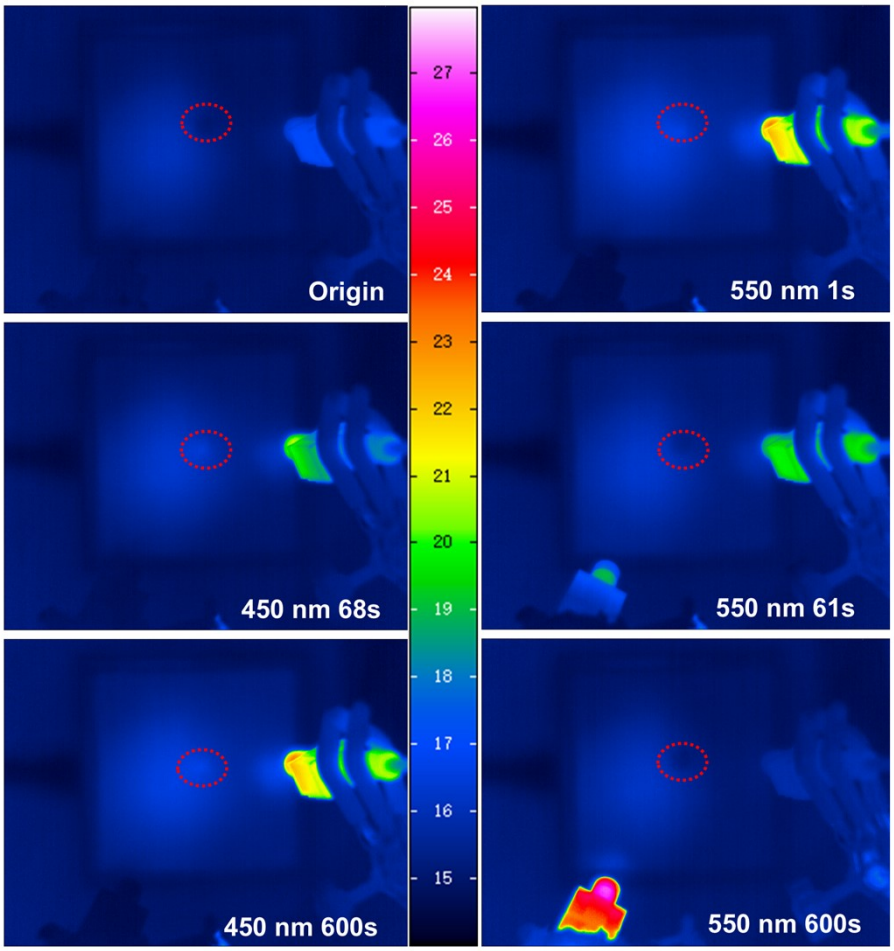

Figure S15. Surface temperature infrared thermal imaging photo of the PSHA-1-Zn photorepair process.

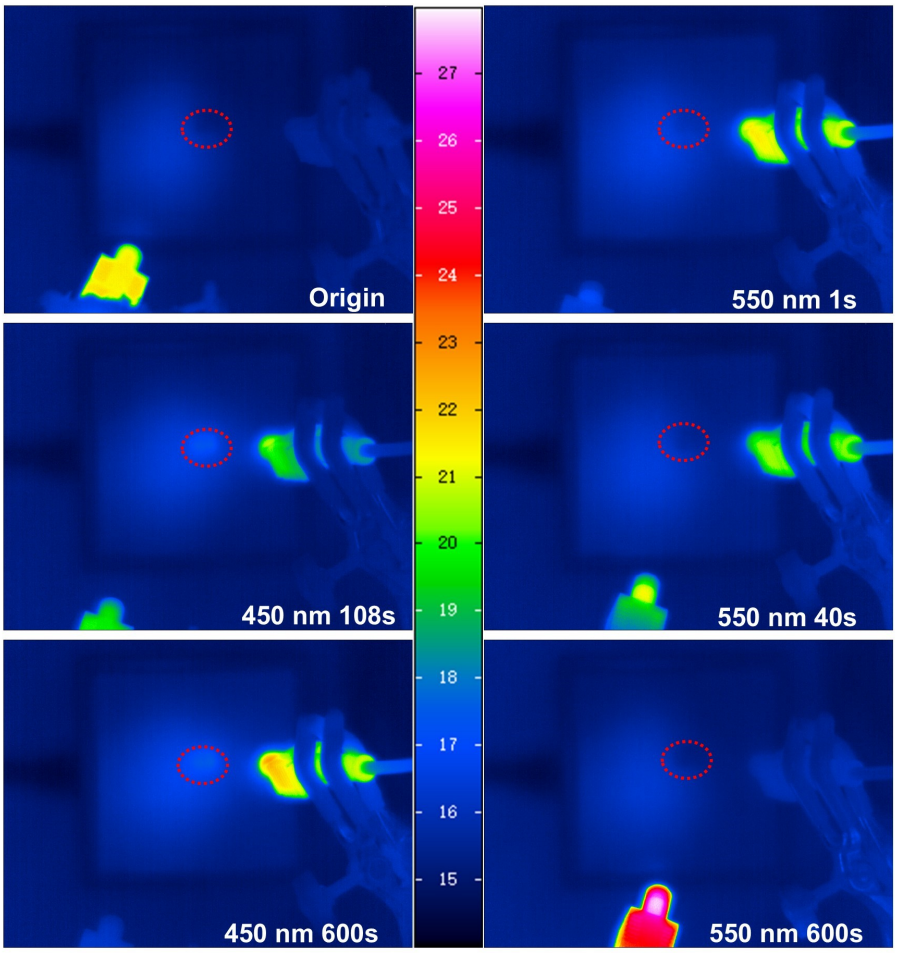

Figure S16. Surface temperature infrared thermal imaging photo of the PSHA-2-Zn photorepair process.

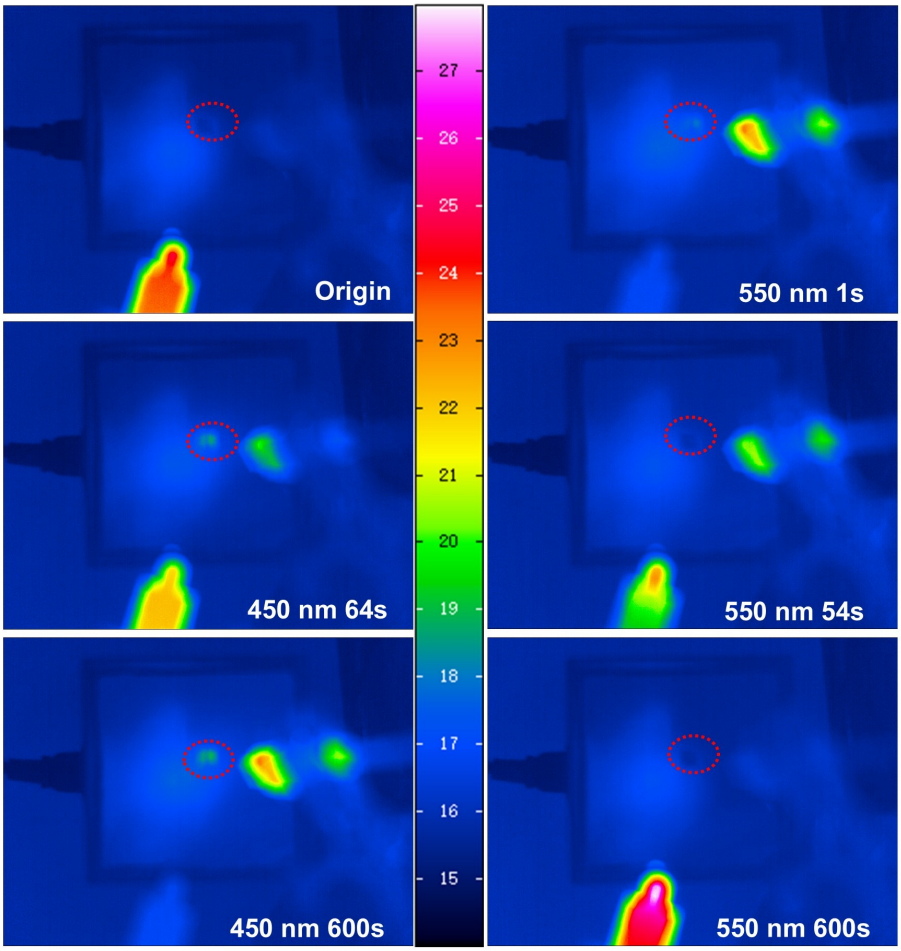

Figure S17. Surface temperature infrared thermal imaging photo of the PSHA-3-Zn photorepair process.

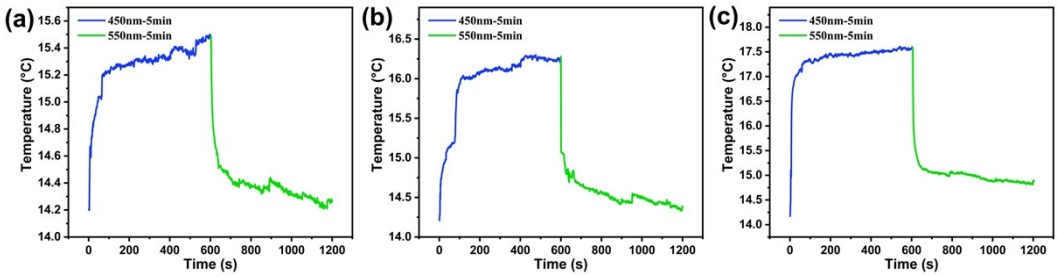

Figure S18. Surface temperature changes during PSHA-Zn simulated light repair process(a)PSHA-1-Zn(b)PSHA-2-Zn(c)PSHA-3-Zn.

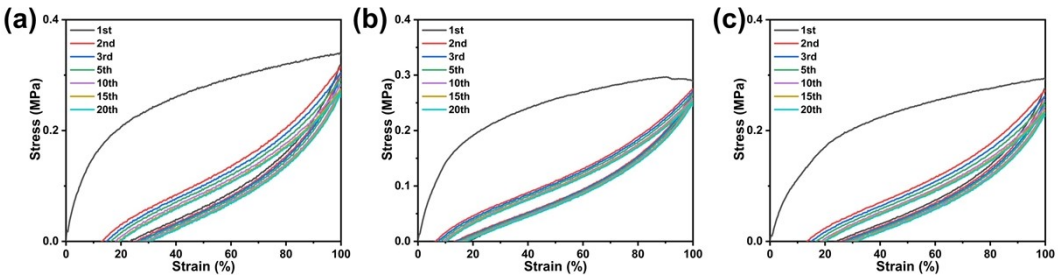

Figure S19. Cyclic stretching curves of PSHA with different THDI contents (a) PSHA-1-Zn, (b) PSHA-1-Zn, (c) PSHA-1-Zn.

Table S5. Detailed data table on light healing under underwater and low-temperature conditions at different times.

Sample	Tensile Stress (MPa)	Tensile Strain (%)	Fracture toughness (MJ/m^3)	Strength healing efficiency(%)	Strain healing efficiency（%）	Toughness healing efficiency(%)
PSHA-1-Zn	0.38 ± 0.02	266.2 ± 13.3	91.02 ± 5.4	-	-	
UWLH-1h	0.36 ± 0.01	110.8 ± 2.5	34.32 ± 0.9	97.1 ± 4.8	48.9 ± 1.2	37.7 ± 0.9
UWLH-2h	0.36 ± 0.03	173.6 ± 7.6	54.68 ± 2.5	96.9 ± 1.8	65.2 ± 1.9	60.0 ± 1.7
-60℃LH-1h	0.33 ± 0.01	101.3 ± 4.1	26.47 ± 0.7	89.3 ± 2.1	38.0 ± 1.7	29.0 ± 0.9
-60℃LH-2h	0.38 ± 0.01	132.7 ± 5.7	43.28 ± 1.5	101.5 ± 2.3	49.8 ± 1.4	47.5 ± 1.4
PSHA-2-Zn	0.43 ± 0.02	415.6 ± 29.0	130.81 ± 3.9	-	-	
UWLH-1h	0.36 ± 0.03	304.6 ± 6.2	80.93 ± 2.2	85.4 ± 1.5	73.2 ± 1.3	61.8 ± 2.2
UWLH-2h	0.42 ± 0.01	403.0 ± 20.7	117.81 ± 5.4	98.2 ± 3.6	96.9 ± 5.0	90.0 ± 1.9
-60℃LH-2h	0.26 ± 0.02	145.2 ± 3.5	26.96 ± 0.9	60.5 ± 1.4	34.9 ± 1.4	20.6 ± 0.8
-60℃LH-4h	0.29 ± 0.01	154.2 ± 7.0	32.73 ± 0.6	68.2 ± 1.1	37.1 ± 0.5	25.0 ± 0.4
PSHA-3-Zn	0.78 ± 0.07	786.7 ± 23.6	385.82 ± 27.0	-	-	
UWLH-2h	0.47 ± 0.03	398.2 ± 7.3	127.92 ± 3.5	60.4 ± 2.3	50.6 ± 1.9	33.1 ± 0.8
UWLH-4h	0.70 ± 0.04	718.6 ± 21.5	315.76 ± 10.3	91.1 ± 2.9	91.3 ± 2.4	81.8 ± 2.7
-60℃LH-1h	0.34±0.01	212.7 ± 3.2	51.63 ± 1.1	44.6 ± 0.9	27.0 ± 1.2	13.3 ± 0.5
-60℃LH-2h	0.44±0.01	323.3 ± 15.3	101.73 ± 3.5	57.0 ± 1.2	41.1 ± 1.1	26.36 ± 1.1

References

1. B. Delley, An all-electron numerical method for solving the local density functional for polyatomic molecules, J. Chem. Phys, 1990, 92, 508–517.
2. B. Delley, From molecules to solids with the Dmol^3 approach, J. Chem. Phys., 2000, 113, 7756-7764.